

## **Heat Transfer through Rockfall**

Ronald T. Green and James D. Prikryl

### **Abstract**

Thermally induced rock stresses at the potential high-level nuclear waste (HLW) repository at Yucca Mountain, Nevada, may degrade the drifts, possibly causing rock rubble to fall onto the dripshield overlying the emplaced waste packages. Thermal-hydrological processes will be altered by changes in thermal conductivity, ventilation, radiation, and convection resulting from such rockfalls. The purpose of this investigation is to measure heat transfer through crushed rock samples of the Topopah Spring lower lithophysal unit at Yucca Mountain as an analog to the rubble and to identify the important heat and mass transfer mechanisms under the expected range of thermal conditions. A laboratory apparatus was used to measure heat transfer through the crushed tuff for temperatures as high as 173°C and thermal gradients as large as 995°C/m. A bulk thermal conductivity value of 0.4 W/m-K was derived from measurements made at low temperatures, low thermal gradients, and low saturation. Empirical relations developed for granular packed bed media suggest that even at elevated temperatures heat transfer by radiation was negligible. Convection, inferred to be that portion of heat transfer not attributed to conduction and radiation, was observed in the experiments at temperature gradients in excess of 600°C/m. Heat transfer by convection through a rubble pile in a HLW emplacement drift, however, are calculated to occur at the much lower temperature gradients expected at the proposed Yucca Mountain geologic repository using a Rayleigh number analysis.

## Introduction

Thermally induced stress at emplacement drifts at the potential high-level nuclear waste (HLW) repository at Yucca Mountain, Nevada, has been shown to cause rockfall into the drift, and possibly onto the drip shield overlying the emplaced waste packages (Gute et al., 2003; Ofoegbu et al., 2004). The transfer of heat through the zone near the degraded emplacement drifts will be altered by changes in thermal conductivity, radiative surface area, and gas and liquid permeability resulting from the rockfall. This will cause the rubble pile to act as a thermal insulator in the zone between the heat source (i.e., HLW canister) and the intact host rock. Determining the impact of rubble on the design of a geologic repository is difficult because heat and mass transfer through the engineered barrier is a complex, coupled process. And the high level of uncertainty in assigning property values to the heterogeneous structure of a rubble pile.

A significant portion of the potential repository at Yucca Mountain as currently designed is in the lower lithophysal unit of the Topopah Spring (Tptpl). Recent laboratory testing of the Tptpl by Brodsky et al. (2003a) provided thermal conductivity measurements of intact samples of the Tptpl rock matrix. Similarly, Brodsky et al. (2003b) has initiated field-scale thermal conductivity measurements of the Tptpl at the Enhanced Characterization of the Repository Block (ECRB) cross drift at the Yucca Mountain Exploratory Studies Facility to account for the volume-average thermal conductivity of the rock, including lithophysae. These two studies provide valuable information on the thermal properties for the Tptpl, but do not provide a measure of these properties for rubble from the Tptpl. Actual rockfall thermal conductivity

values could vary outside the range of values bracketed by the laboratory- (Brodsky et al., 2003a) and field- (Brodsky et al., 2003b) scale measurements.

Transient and steady-state methods are available for measuring thermophysical properties. Both classes of methods have strengths and weaknesses. Transient methods are used to estimate thermal diffusivity and require shorter heating periods than steady-state methods (Singh and Chaudhary, 1992). Conversely, steady-state methods allow unambiguous determination of thermal conductivity, while transient methods require an independent estimate of heat capacity in order to determine thermal conductivity from thermal diffusivity measurements. Because the heat transfer processes at a geologic repository are expected to vary slowly, transient thermal effects are assumed to be of secondary importance compared to the steady-state transfer of heat. Thermal conductivity (or effective thermal conductivity), not heat capacity or thermal diffusivity is, therefore, the primary focus of this investigation.

The purpose of this investigation is to assess the thermal properties of an analog rubble pile and identify the important heat and mass transfer mechanisms anticipated to be active under quasi-steady-state conditions in rubble collapsed around HLW canisters for conditions expected at a potential geologic HLW repository. To accomplish this objective, a steady-state laboratory apparatus was used to directly measure the bulk thermal conductivity of crushed rock for a range of temperatures. The laboratory method used in these experiments closely paralleled the methodology developed by Green et al. (1997). Laboratory experiments and analyses were conducted to investigate the various heat transfer mechanisms that might be active in a rubble pile expected in emplacement drifts (Gute et al., 2003; Ofoegbu et al., 2004). Analyses were

conducted to identify the range of thermal-physical conditions over which the various heat transfer mechanisms would be active.

### **Background**

Heat will be transferred by conduction, convection, and radiation from HLW canisters to the drift walls of a geologic repository. The relative importance of the heat transfer processes could remain constant under stable drift conditions, or they could be significantly altered in the event that rockfall covers the drip shield overlying the canisters. Heat transfer mechanisms would change due to the rubble pile acting as an insulator and the alteration of the free air space available for heat transfer by radiation and convection.

At relatively low temperatures, heat transfer through either intact rock or rubble at the potential repository will probably occur by conduction only. Convection and radiation are expected to contribute to the total heat flow only at high temperatures or high temperature gradients. For circumstances with limited information, an effective thermal conductivity value that represents all active heat transfer mechanisms can be assigned to the medium for a specified range of conditions (Kaviany, 1995). This approach, however, may violate Fourier's law of heat conduction which assumes a linear relationship between heat flux and temperature gradient. Nonetheless, assuming an effective thermal conductivity is often expedient and, in reality, the only option.

Heat transfer through rockfall at higher temperatures may be enhanced if a heat pipe develops. Heat pipes are highly efficient heat transfer mechanisms in which coupled evaporation, condensation, latent-heat transfer, and capillary-driven return flow of liquid remove heat at higher rates than normally experienced by conduction and convection (Mills, 1995). A heat-transfer mechanism similar to a heat pipe may form in the fractured, porous media near a heat-generating HLW canister. In this mechanism, which is commonly referred to as counter current, the return flow of water is driven by gravity, rather than by capillary forces active in a heat pipe.

The rock unit under consideration is the Tptpl. The texture and strength of the Tptpl will affect drift integrity and how the rock breaks after failure. For example, heat transfer through large pieces of brittle rock will differ from heat transfer through crushed rock with lithophysae and a large portion of powder and fine-grained material. Evaluation of heat transfer through rockfall that may occur at the potential HLW repository at Yucca Mountain, therefore, is performed on the actual host rock, (i.e., the Tptpl).

Actual heat transfer through a rubble pile will depend on the physical properties of the native rock (i.e., fragment size distribution and packing) and thermal-hydrological conditions (i.e., temperature, temperature gradient, and saturation) encountered. The fragment size distribution and packing expected in the rubble pile are uncertain; however, it is reasonable to expect that some rubble pile fragments may be larger than those used in these experiments.

The heat transfer measurements conducted on the relatively small-size fragments used in this study may not be directly applicable to rubble with many large fragments; however the tests have relevance because the rock sample is from the Tptpll and has been crushed. The assumption of low saturations used in this analysis is considered appropriate because the rubble pile will likely have low saturation due to long durations (i.e., hundreds to thousands of years) of heating expected for the repository as currently designed (DOE, 2004). This assumption may not be valid for situations where the rubble saturation is increased by seepage or focused recharge.

### **Previous Measurements of Thermal Conductivity**

Measurements and estimates of the thermal conductivity of intact rock at Yucca Mountain have been made by numerous investigators (Lappin, 1980; Lappin et al., 1982; Sass and Lauchenbruch, 1982; Lappin and Nimick, 1985; Nimick and Lappin, 1985; Sass et al., 1988; Nimick, 1990a,b; Brodsky et al., 2003a,b). The *in situ* texture of the Tptpll introduces challenges when attempting to assign representative property values, in general, and thermal conductivity values, in particular. The large proportion of voids and the heterogeneous distribution of lithophysae in the Tptpll make characterization difficult. Sufficiently large representative elemental volumes (Bear, 1972) need to be sampled to provide representative measurement of the intact Tptpll.

Recent laboratory- and field-scale experiments were conducted on the Tptpll to provide insight on the thermal conductivity of intact rock. A guarded heat flow meter was used by Brodsky et al. (2003a) to measure thermal conductivity of the rock matrix at the laboratory scale. Intact matrix

samples of the Tptpl unit were collected from surface-drilled boreholes and from boreholes drilled into the sidewall of the ECRB cross drift. The thermal conductivity of specimens ranging in size from 38.1 to 50.8 mm in diameter and 6.35 to 12.7 mm in height was measured during the testing. Thermal conductivity measurements of these test specimens were made at both dry and fully saturated conditions at temperatures that ranged from 30 to 175 °C. The effect of porosity was evaluated by drilling holes into the test specimens to create additional porosity as a controlled surrogate for lithophysal porosity. The average value of thermal conductivity was  $1.7 \pm 0.2$  W/m-K for oven-dried samples and  $2.1 \pm 0.2$  W/ m-K for fully saturated samples. There was no measurable difference in thermal conductivity between the different sized samples. Increased porosity had the effect of decreasing thermal conductivity for test specimens measured at constant saturation and increasing the difference in thermal conductivity of samples measured at different saturation levels (Brodsky et al., 2003a).

Field-scale thermal conductivity testing was conducted in boreholes drilled into the sidewall of the ECRB (CRWMS M&O, 2001; Brodsky et al., 2003b). In these tests, a 5-m long heater was inserted in a borehole and energized at 433 W for nearly 30 days. The thermal response of the intact rock was measured in an adjoining borehole. Approximately 100 to 200 m<sup>3</sup> of intact rock was heated above the ambient temperature during each test. The field-scale thermal conductivity test program was conducted at low power to insure the measurements were made at temperatures below boiling. All tests were conducted at *in situ* moisture conditions. Thermal conductivity was estimated by heating the intact rock mass with the heater placed in one borehole and measuring the evolution in temperature at an adjoining borehole. The heater was placed in a horizontal borehole at a 45-degree angle relative to the wall of the ECRB. Temperatures were measured at

30 locations in a 5-m section of an adjoining horizontal borehole oriented perpendicular to the heater cartridge. The instrumented borehole was positioned 16-cm (center to center) above the heater borehole. This provided a minimum of 8.4 cm of rock between the two boreholes. The bulk *in situ* thermal conductivities at two locations in the ECRB were 1.7 to 1.8 W/m-K and 2.0 to 2.2 W/m-K.

The rubble pile associated with drift collapse would most probably be a heterogeneous mixture of partially crushed rock. Ryder et al. (1996) conducted a bench-scale experiment to measure the effective thermal diffusivity of crushed welded tuff. A range in effective thermal conductivity of 0.58 to 0.74 W/m-K was determined by assuming representative values for heat capacity, porosity, and bulk permeability for several different expressions that relate thermal diffusivity and thermal conductivity.

Measurement of the thermal properties of the Tptpl as rubble will differ from intact rock as suggested by the following studies. Connor et al. (1997) conducted field-scale tests to evaluate *in situ* heat and mass transfer through scoria, where a recently emplaced igneous dike provided the source of heat. The scoria in the dike zone was determined to have a bulk thermal conductivity of  $\sim 0.2$  W/m-K based on representative values for heat capacity, porosity, and bulk permeability. This value is approximately one order of magnitude less than measured thermal conductivity of dense basalt (Connor et al., 1997). Green et al. (1997) conducted laboratory-scale tests to measure bulk thermal properties of crushed welded tuff (i.e., Apache Leap tuff) from the Apache Leap Test Site in Superior, Arizona, over a range of temperatures, temperature gradients, and saturation levels. The thermal conductivity of the crushed welded tuff was measured to be

0.49 W/m-K compared with the thermal conductivity of intact Apache Leap tuff which was measured to be 1.74 to 1.91 W/m-K (Green et al., 1995).

## Theory

Heat can be transferred through rockfall by conduction, convection, and radiation. Because any of these heat transfer modes can contribute to heat transfer for at least a portion of the range of possible conditions at a HLW repository, all mechanisms will be considered *a priori*. The heat transfer mechanisms are defined as follows.

### Conduction

Heat transfer by conduction is assumed to obey Fourier's law

$$q_{cond} = -\kappa_T \nabla T \quad (1)$$

where  $q_{cond}$  is heat flow per unit area ( $\text{W}/\text{m}^2$ ),  $\kappa_T$  is the thermal conductivity ( $\text{W}/\text{m}\cdot\text{K}$ ), and  $T$  is temperature. For a conduction-dominated system where boundary temperatures and heat flux are known, thermal conductivity can be directly calculated.

### Radiation

Radiation is an electromagnetic phenomenon in which energy is transmitted through space from a heated source. Thermal radiation travels easily through a vacuum, less easily through gasses and liquids, and not at all through solids, with the possible exception of glass and clear plastic. A heated surface emits radiant energy,  $E_{rad}$ , at a rate that is proportionate to the fourth power of the absolute temperature of the surface according to the following relation

$$E_{rad} = \varepsilon \sigma A T^4 \quad (2)$$

where  $\varepsilon$  is emissivity, which accounts for that fraction of maximum radiation actually emitted from the surface,  $\sigma$  is the Stefan-Boltzmann constant ( $5.67 \times 10^{-8} \text{ W/m}^2\text{-K}^4$ ), and  $A$  is area from which radiant heat is emitted. The radiant energy flux is

$$q_{rad} = -\varepsilon \sigma T^4 \quad (3)$$

The effect of porous media on radiative transport has been accommodated by modifying Equation (3) to the following (Botterill et al., 1989)

$$q_{rad} = -4\chi d_p \sigma T^3 \nabla T \quad (4)$$

where  $d_p$  is the mean particle size, and  $\chi$  is a radiation transfer function, which is a function of the particle surface emissivity and the assumed radiative transfer geometry. The value of  $\chi$  is a function of the unit cell model (i.e., radiative transfer geometry) assumed to represent the porous media. A summary of the unit cell models is given by Botterill et al. (1989). Values of  $\chi$  for these unit cell models vary from 0.29 to 1.65 for alumina and from 0.279 to 1.377 for silica (Botterill et al., 1989). The variation is due to the different values assigned to porosity (i.e., unit cell model) and emissivity.

### **Convection**

Convection can be described as the transfer of heat by conduction in a fluid as enhanced by the motion of the fluid (White, 1988). The driving forces of the liquid phase are assumed to be dominated by gravity, capillarity, and surface forces, except for fully saturated conditions.

Buoyancy from density variations would be the dominant driving force when the fluid is fully saturated or in the gas phase. Systems that are sufficiently permeable and demonstrate a large temperature gradient can lead to self-driven convection cells. The onset of convection is experienced when the Rayleigh number, a dimensionless ratio of buoyancy to viscous

retardation, exceeds a critical value. The Rayleigh number for porous media is defined as follows (Witherspoon et al., 1975)

$$Ra = \frac{k \rho^2 g \beta \Delta T C_v D}{\mu \kappa_{eff}} \quad (5)$$

where  $k$  is permeability ( $m^2$ ),  $g$  is acceleration due to gravity ( $m/s^2$ ),  $\beta$  is the coefficient of volumetric expansion ( $K^{-1}$ ),  $\Delta T$  is the difference in temperature between the bottom and top boundaries,  $C_v$  is specific heat at constant volume ( $J/kg\cdot K$ ),  $D$  is the depth of the convection cell ( $m$ ),  $\mu$  is viscosity ( $kg/m\cdot s$ ),  $\rho$  is fluid density ( $kg/m^3$ ), and  $\kappa_{eff}$  is the effective thermal conductivity ( $J/m\cdot K\cdot s$ ). For conditions where the Rayleigh number exceeds a critical value, referred to as the critical Rayleigh number, natural or free convection occur. In porous media, the critical Rayleigh number,  $Ra_{cr}$ , equals  $4\pi^2$  (Lapwood, 1948). Heat flux by convection can be expressed in terms of an effective thermal conductivity by the following (Witherspoon et al., 1975):

$$q_{conv} = -c_{conv} Ra^{\frac{1}{4}} \nabla T \quad (6)$$

where  $c_{conv}$  is an experimentally determined fitting parameter. Because  $Ra$  is proportional to the temperature gradient, this expression can be simplified to

$$q_{conv} = -c_{conv}^* (\nabla T)^{\frac{5}{4}} \quad (7)$$

where the fitting parameter is modified to include  $Ra^{\frac{1}{4}}$ . Lastly, Equation (7) is modified to account for the minimum temperature gradient required for the onset of convection

$$q_{conv} = -c_{conv}^* \left[ (\nabla T)^{\frac{5}{4}} - (\nabla T_{critical})^{\frac{5}{4}} \right] \quad (8)$$

where  $(\nabla T)_{critical}^{5/4}$  is the critical temperature gradient that must be exceeded for convection to occur.

### **Total Heat Flux**

Total heat transport can be defined by summing the conduction, radiation, and convection components

$$q_{total} = -\kappa_T \nabla T - \chi d_p \sigma 4T^3 \nabla T - c^*_{conv} \left( (\nabla T)^{\frac{5}{4}} - (\nabla T_{critical})^{\frac{5}{4}} \right) \quad (9)$$

### **Description of Thermal Conductivity Test Apparatus**

A laboratory apparatus was used to measure the steady-state transfer of heat through crushed Tptpll under a variety of thermal conditions. The experiments were conducted under steady-state conditions to avoid the added uncertainty that derives from the need to determine values for density,  $\rho$ , and specific heat,  $C_p$ , which are required when extracting thermal conductivity values,  $\kappa_T$ , from thermal diffusivity measurements.

The steady-state thermal heat flux apparatus was designed to established only vertical heat flow through the centrally located  $0.15 \times 0.15 \times 0.15$  m volume of tested material. The material placed outside of the centrally located tested material was added to ensure vertical heat flow conditions and avoid potential deleterious effects of heat loss or gain through the outer boundary. This design avoids the need to emplace thermocouples in the test specimen to document that heat flow is indeed only vertical, a procedure that could cause measurement errors because of high thermal conduction through the thermocouples. Difficulties of this nature have been encountered

when using alternative experimental designs (Ryder et al., 1996). A photograph of the steady-state apparatus is shown in Figure 1, and a schematic diagram is illustrated in Figure 2.

The apparatus consists of a  $0.9 \times 0.9 \times 0.15$  m cell designed to accept bulk test specimens. Two 2.5-cm thick aluminum plates form the top and bottom of the test cell. The test sample is held under a slight compressive load (nine compressive bolts tightened to 6.8 Newton-meters) between two 2.54 cm-thick aluminum plates. The aluminum plates were temperature controlled with a uniform heat source applied to the lower boundary and a liquid cooled heat sink built into the upper aluminum plate. The apparatus will accommodate dry to fully saturated samples over a temperature range of 10 to  $230^{\circ}\text{C}$ ; however, only unsaturated samples were considered during these tests.

Calibrated Micro-Foil<sup>TM</sup> heat flux sensors (with a maximum recommended heat flux of  $95,000 \text{ W/m}^2$ ) were placed at the corners of  $0.15 \times 0.15 \times 0.0023$  m depressions milled into both the upper and lower plates to allow for measurement of the heat flux ( $\text{W/m}^2$ ) into and out of the test specimen. A K-Type thermocouple (with a recommended range of  $-330$  to  $2300^{\circ}\text{C}$ ) was mounted in each heat flow sensor to measure temperature. The remaining volume of material was included to ensure only vertical heat flow occurs in the central portion of the cell. Thus, heat flow was only measured through the centrally located  $0.15 \times 0.15 \times 0.15$  m volume of the chamber, which equates to  $0.0034 \text{ m}^3$  compared with the total volume of the chamber (i.e.,  $0.12 \text{ m}^3$ ).

In addition to the thermocouples contained in each heat flux sensor, temperature was measured at four points near the edges of both the lower and upper aluminum plates to measure the test cell boundary conditions. These T-Type thermocouples were placed midway along each side of the aluminum plates to measure the uniformity of temperature throughout the upper and lower boundaries. No instrumentation was placed in the test medium within the cell to avoid the possibility of a pathway for heat transfer that would distort the steady-state thermal measurements. Heat flow and temperature measurements were taken every 10 to 20 minutes for the duration of each test and recorded with an automatic data acquisition system. The test apparatus, therefore, measured the temperature gradient and heat flux through the test specimen allowing calculation of the thermal conductivity of the bulk sample material.

### **Description of Test Specimen**

The Tptpl is a moderately to densely welded, devitrified, and vapor-phase altered tuff (Mongano et al., 1999). As characterized in the Cross-Drift Exploratory Studies Facility, the Tptpl is composed of 3 to 7 percent pumice, 1 to 2 percent phenocrysts, 1 to 5 percent lithic fragments, 5 to 30 percent lithophysae, and 56 to 90 percent matrix (Mongano et al., 1999). Throughout most of the unit, vapor-phase spots, stringers, and wisps comprise between 3 and 12 percent of the rock. In several intervals, however, vapor-phase alteration products form 15 to 40 percent of the rock. Lithophysae vary in size, shape, and abundance throughout the zone. For ease of description, the lower lithophysal zone has been divided into seven intervals with generally similar lithophysae size and abundance (Mongano et al., 1999). These interval boundaries do not have stratigraphic significance. The moderately to densely welded matrix of the lower

lithophysal zone is a mix of devitrified and vapor-phase altered material. Throughout most of the zone, shard texture has been destroyed by secondary crystallization. An exception occurs near the base of the zone where silicification locally preserves shard texture.

Samples of the Ttppll were collected from the muck pile at the end of the conveyor used during the excavation of Niche No. 5 in the ECRB at Yucca Mountain. Sufficient samples of the Ttppll were collected to fill six metal 55-gallon barrels. No effort was made to select size fractions while filling the barrels. The six barrels were mechanically sealed and delivered to Southwest Research Institute® in San Antonio, Texas.

A bulk sample of Ttppll muck was removed from one of the drums and placed into the thermal conductivity test cell. Rock fragments with a diameter greater than 6 cm were not used. No effort was made to control the moisture content of the rock samples during loading of the sample or the performance of the tests. The temperature of the laboratory was between 20 to 25°C from the time the drums were received to the conclusion of the experiments. The relative humidity was less than 30% during this same period. The rock is expected to have dried significantly during the 3 months from the time of mining to the start of the experiments because of exposure to relatively low humidity and high temperature air combined with the mining-induced large surface area of the specimen. With the exception of Test 1, as explained in the test results section, the thermal conductivity values measured during these tests are believed to be approximately representative of dry thermal conductivity values.

## Laboratory Procedure

A total of 12 tests was conducted on the same sample of Tptpl. The tests were conducted under different temperature regimes to determine whether the transfer of heat is sensitive to variations in the temperature and temperature gradient. Heat flux was controlled at the lower and upper boundaries by varying the temperature difference between the aluminum plates (e.g., increasing or decreasing the temperature of the heater at the bottom boundary, the heat sink at the top boundary, or both) during the tests. The bottom and top temperatures and resulting temperature gradients for each test are summarized in Table 1.

### Description of Tests

Good thermal connectivity between the bulk test specimen and the lower aluminum plate was provided by the fine-grained material that sifted to the bottom of the test cell during emplacement of the sample in the cell. The potential for insufficient thermal connectivity between the bulk test specimen and the upper aluminum plate (heat sink) was avoided by placing a pliable layer of crumpled tin foil on top of the tuff samples prior to emplacement of the top plate. The tin foil acted to minimize the possible thermal resistance resulting from poor thermal connectivity (i.e., excessive air gaps) between the rock sample and the top plate. Temperature and heat flux measurements for the top and bottom boundaries reported in Table 2 are averages of the four heat flux and temperature measurements located in the central  $0.15 \times 0.15$  m areas of the top and bottom aluminum plates.

The time to steady state in the experiments was estimated by calculating the time required to raise the temperature of the test sample from the initial temperature to the final temperature

given the heat flux imposed at the bottom boundary. The time required to raise the initial temperature of the test sample to the final temperature was estimated using the following equation:

$$t_{steadystate} = \frac{A}{q} \left[ \frac{(T_{bottom}^{final} - T_{top}^{final})}{2} + \frac{(T_{bottom}^{initial} - T_{top}^{initial})}{2} \right] C_p M_{rock} \quad (10)$$

where  $A$  is the cross-sectional area of the test cell,  $C_p$  is specific heat (J/kg-K),  $M_{rock}$  is the mass of the test medium (kg), and  $q$  is the heat flux measured at the bottom boundary. This calculation assumes that all heat entering the test volume is measured by the bottom heat flux sensors remained in the test specimen. The actual times needed to attain steady state in the tests were somewhat greater than this estimate because the heat was removed from the system at the upper boundary heat sink before the entire test specimen attained the final desired temperature distribution. Nonetheless, this estimate provided a first-order approximation of the elapsed time required before a valid measurement could be made.

To estimate the time required to approximate steady-state conditions, a specific heat of 840 J/kg-K was assigned to the crushed Tptpl. The mass of the test medium was determined to be 165 kg. Although initial temperatures in the experiments were dependent on the final temperature of the preceding experiment, the maximum increase in temperature from one test to the next was no greater than the 55°C difference observed between Tests 9 and 10. The heat flux at the bottom boundary was measured at 186.6 W/m<sup>2</sup> during Test 10. The time for steady-state temperatures to be achieved was estimated to be about 9.2 hours. During conduct of the tests, a minimum of 48 hours was allowed for each test to attain steady-state temperatures. In addition, all experiments were continued until both the lower and upper heat flux measurements became

steady, a condition that was realized in all 12 tests. The assumption of steady-state heat flux conditions, therefore, was justified for all tests.

### **Laboratory Results**

The contributions of conduction, convection, and radiation to heat transfer are estimated using the test results and the relationships stated above. The contribution of heat transfer by conduction is estimated using data from low temperature gradient experiments. The contribution to heat transfer by radiation is calculated based on measured temperature and estimated particle size. The contribution to heat flux by convection is assumed to be that portion of the measured heat flux that remains after conduction and radiation are removed.

Boundary temperatures in the 12 tests ranged from 37.6 to 173.4°C at the bottom and 5.1 to 24.2°C at the top. The difference in temperature between the top and bottom varied from 23.6 to 149.3°C with a temperature gradient that ranged from a low of 157.1 to a high of 995.3°C/m. Heat flux averaged from measurements varied from 52.4 to 509.3 W/m<sup>2</sup> at the bottom and 58.1 to 429.5 W/m<sup>2</sup> at the top. The apparent thermal conductivity for the tests is illustrated in Figure 3, a plot of heat flux versus temperature gradient. The standard deviation of heat flux measured by the 8 (4 upper and 4 bottom) sensors is included in Figure 3 for all 12 tests. The data exhibit a linear trend at low temperature gradients with a deviation from linearity at higher temperature gradients (i.e., > 500°C/m) and heat flux (i.e., > 250 W/m<sup>2</sup>). The deviation from linearity, however, does not exceed the standard deviation of measurements until the temperature

gradient exceeds  $800^{\circ}\text{C}/\text{m}$  and the heat flux exceeds  $400\text{ W}/\text{m}^2$ . This departure suggests radiation and convection are active at higher temperature gradients.

### **Conductivity**

Heat transfer is assumed to have occurred exclusively by conduction in tests conducted at low temperature gradients. The thermal regime at which conduction is the dominant heat transfer mechanism is that regime where the relationship between heat flux and the temperature gradient is linear, as described by Fourier's law [Equation (1)]. The linear relationship up to a temperature gradient of  $500^{\circ}\text{C}/\text{m}$  or a heat flux of  $250\text{ W}/\text{m}^2$  is illustrated by the straight line in Figure 3. The slope of the line approximating the linear portion of the data (up to a temperature gradient of  $500^{\circ}\text{C}/\text{m}$ ) indicates a thermal conductivity of  $0.4\text{ W}/\text{m}\cdot\text{K}$  for the multi-sized test specimen.

### **Radiation**

The contribution to heat transfer by radiation is calculated for the range of temperature gradients observed during the tests (i.e., as great as  $995.3^{\circ}\text{C}/\text{m}$ ) using Equation (4) and assuming  $\chi = 1$ .

The material comprising the test specimen cannot be characterized with a single diameter; therefore, radiation was calculated for particle diameters that range from  $0.00001$  to  $0.06\text{ m}$ . The calculated heat transfer due to radiation in media with these diameters is presented in Figure 4. Heat transfer calculated for particles with diameters of  $0.00001$  to  $0.001\text{ m}$  is also presented in Figure 5 for clarity of the lower radiation heat flux values associated with smaller particles. The contribution to heat flux by radiation in these tests was negligible (i.e.,  $< 5\text{ W}/\text{m}^2$ ), except when the thermal gradient exceeded  $600^{\circ}\text{C}/\text{m}$  and the particle size exceeded  $0.001\text{ m}$ . The cumulative effect of the mixture of particle sizes in the test specimen is hypothesized to transfer heat by radiation consistent with smaller, uniform-sized particles compared with larger, uniform-sized particles. For material with the size distribution of the test specimen, heat flux by radiation is

determined to be negligible (i.e.,  $< 2 \text{ W/m}^2$ ) even at larger (i.e.,  $> 600^\circ\text{C/m}$ ) temperature gradients primarily because of the mixed-size distribution of the test specimen. The mixed-size distribution provides fewer voids, thereby limiting the potential for heat transport by radiation. Heat transfer by radiation is, therefore, considered negligible for the thermal regimes and material under consideration.

### **Convection**

The contribution of convection to heat transfer is calculated by subtracting the conduction component (e.g., calculated for  $\kappa_T = 0.4 \text{ W/m-K}$ ) from the overall heat transfer observed and assuming that heat transfer by radiation is negligible. The resulting values for heat flux by convection are presented in Table 3 and plotted versus  $(\nabla T)^{5/4}$  in Figure 6. As illustrated, convection was only active when the temperature gradient exceeded 500 to  $600^\circ\text{C/m}$  [comparable to  $(\nabla T)^{5/4} = 2364\text{--}2969$ ]. The critical temperature gradient required for the onset of convection is set at  $\nabla T = 572^\circ\text{C/m}$  [i.e.,  $(\nabla T)^{5/4} = 2800$ ]. Above this temperature gradient, it appears that heat flux by convection increased approximately linearly versus  $(\nabla T)^{5/4}$  over the  $(\nabla T)^{5/4}$  range of 2800 to 6000. To demonstrate this trend more clearly, only data from tests with  $(\nabla T)^{5/4}$  greater than 2800 are plotted in Figure 7. The resulting linear relationship is consistent with the  $(\nabla T)^{5/4}$  power relationship indicated in Equation (8).

The datum from Test 1 is an outlier in Figures 3 and 6. The quantity of heat transfer remaining after the subtraction of heat transfer by conduction in Test 1 is significantly greater (i.e.,  $41.4 \text{ W/m}^2$ ) relative to the imposed temperature gradient [i.e., 2680 when expressed as  $(\nabla T)^{5/4}$ ] when compared to the other data. A possible source of this discrepancy is that the saturation of the specimen was greater at the onset of testing than previously thought. A higher

initial saturation would have provided a larger thermal conductivity not representative of the drier thermal conductivity values measured during Tests 2–12.

Convection fitting parameters for each test calculated using Equation (8) are summarized in Table 3 and plotted versus  $(\nabla T)^{5/4}$  in Figure 8. The fitting parameters are near zero (i.e., less than  $\pm 0.005$ ) for  $(\nabla T)^{5/4}$  less than 2800 and relatively constant at 0.024 to 0.027 for Tests 6, 7, 11, and 12, where  $(\nabla T)^{5/4}$  is greater than 2800. Two exceptions to these trends are Test 1 (previously discussed and not plotted in Figure 8) and Test 5 with a convection fitting parameter of 0.076. The cause for the anomalously high value of 0.076 in Test 5 is not known; however, the 0.024 to 0.027 values for the four other tests sufficiently similar for the range of  $(\nabla T)^{5/4}$  greater than approximately 3600 that a constant value of 0.024 to 0.027 is believed to be appropriate for the convection fitting parameter.

Convection cell formation (i.e., number and dimension of cells) is dependent on the temperature gradient in the test specimen and the geometry of the test cell as defined by the Rayleigh number in Equation (5). Multiple convection cells may have formed in the test cell with a 6:1 horizontal to vertical dimension ratio. Additionally, pathways of the gas phase may have varied among the tests because of their different temperature regimes. However, because all tests were conducted on the same packing of the same test specimen under similar saturation conditions (with the possible exception of Test 1) and not dramatically different thermal conditions, it is believed that the convection cells were similar for all tests, albeit at different strengths.

The Rayleigh number calculated for the test cell and specimen provides corroborating evidence that convection might have contributed to heat transfer for the conditions at which testing was conducted. With the exception of permeability, minimal uncertainty is associated with the values assigned to the variables in Equation (5). Assuming that the test specimen has a permeability value of  $1.0 \times 10^{-7} \text{ m}^2$ , appropriate for coarse gravel (Freeze and Cherry, 1979), the test has a Rayleigh number of 35.7 with a  $50.0^\circ\text{C}$  temperature difference between the lower and upper plates (equivalent to a temperature gradient of  $333^\circ\text{C/m}$ ). This Rayleigh number value is comparable to the critical Rayleigh number of  $4\pi^2 (= 39.5)$ , indicating that air convection could be a contributor to heat transfer for tests with a temperature gradient in excess of about  $350^\circ\text{C/m}$ .

Inspection of the estimated convection values in Table 3 suggests that convection was active during Tests 5, 6, 7, 11, and 12 and possibly Tests 1 and 10. Each of these tests had a temperature gradient of at least  $588^\circ\text{C/m}$ . Conversely, tests without appreciable convection had temperature gradients no greater than  $454^\circ\text{C/m}$ . Temperature gradients in the range of  $454$  to  $588^\circ\text{C/m}$  are in the zone of transition where the onset of convection is experienced. The temperature gradient indicating the regime when convection is active was marginally greater than the minimum temperature gradient required for convection calculated with Equation (5) (i.e.,  $350^\circ\text{C/m}$ ).

The measured heat flux at the bottom and top heat flux sensors is compared with the calculated heat transfer by convection in Table 3. A slightly higher heat flux is observed at the bottom boundary compared with the top boundary at lower average temperatures, and a significantly higher heat flux is measured at the top boundary compared with the bottom boundary at higher

average temperatures. The component of total heat flux attributed to convection (Table 3) in the aforementioned analysis is comparable with the quantity of heat flux measured at the top boundary that is in excess with that measured at the bottom boundary.

### **Estimate of Heat Transfer through Rockfall in an Emplacement Drift**

Recent analyses by Gute et al. (2003) and Ofoegbu et al. (2004) suggest that emplacement drifts may experience rockfall during the period when heat is generated by the HLW canisters.

Although uncertainties exist in the timing of the rockfall and the texture of the rubble pile, these materials would alter the transfer of heat from the surface of the drip shield if sufficient rubble were to collapse onto the drip shield (Figure 9). If the Tptpl rubble pile encountered in the Yucca Mountain emplacement drifts is similar to the Tptpl muck specimen tested during this study, the rubble pile would have a thermal conductivity of 0.4 W/m-K.

Heat transfer by radiation through the rubble pile is expected to be negligible unless the rubble pile consists of large angular pieces with minimal fine-grained material filling air voids. Rubble of this type is not expected in the Tptpl unit; however, future assessments may indicate that rubble piles have sufficiently large air gaps. If this is the case, radiation should be reconsidered.

The onset of convection in emplacement drifts that experience rockfall is expected when the Rayleigh number for the collapse zone exceeds the critical Rayleigh number. In addition to the temperature gradient, two physical characteristics will affect the Rayleigh number of the collapse zone and the critical Rayleigh number: (i) the increased height of convection cell in emplacement

drifts that experience rockfall and (ii) the aspect ratio of the width to height of collapsed emplacement drift.

The Rayleigh number will increase linearly with the height of the collapse zone based on the assumption that the height of the convection cell is equivalent to the height of the collapsed zone. Consequently, convection may occur in the collapse zone at temperature gradients smaller than observed during the laboratory-scale experiments because of the increased height of the convection cell.

The critical Rayleigh number equals  $4\pi^2$  when the aspect ratio of width to height of the collapse zone is unity. Gute et al. (2003), however, noted that the emplacement drift aspect ratio may not be unity, particularly when stoving is experienced (Figure 9). In particular, the critical Rayleigh number increases with a decrease in the aspect ratio according to the following (Donaldson, 1970)

$$Ra_{CR} = \pi^2 \frac{m^2 + S^2}{m^2 S^2} \quad (11)$$

where  $S$  is the aspect ratio and  $m$  is the largest integer less than

$$1 + \left[ -\frac{1}{2} + \frac{1}{2} (1 + 4S^2)^{\frac{1}{2}} \right] \quad (12)$$

Based on this expression,  $m$  equals 1 for an aspect ratio of .1 to 1, which encompasses the range of interest for this evaluation. The critical Rayleigh number is plotted versus the drift height in Figure 10. As illustrated, the critical Rayleigh number only exceeds 50 when the aspect ratio is less than 0.6.

Estimating the cell height in the collapse zone above the waste package and using material property values included in the definition of the Rayleigh number that were measured at laboratory scale during this investigation allows estimation of what temperature gradients would be required for heat transfer by convection to occur in emplacement drifts that experience rockfall. Gute et al. (2003) estimated the drift degradation zone height to be 10 to 40 m based on various bulking factors. This suggests an aspect ratio of 0.5 (equivalent to a height of 10 m) to 0.125 (equivalent to a height of 40 m) if the drift width is assumed to remain constant at 5 m. The critical Rayleigh number varies from 61 to 650 over this range of aspect ratio.

A Rayleigh number for an emplacement drift that has experienced rockfall is calculated using the property values determined for the Tptpl test specimen tested during this study. The Rayleigh number for a modest temperature difference of 50°C between the heat package located at the base of the emplacement drift and the top of the collapse zone is plotted in Figure 11.

Temperature differences in intact emplacement drifts at the proposed Yucca Mountain geologic repository are expected to exceed this modest level for periods up to several thousand years in intact emplacement drifts (DOE, 2004). Similarly, temperature differences expected for the rubble pile are uncertain, but are also expected to exceed this modest level.

As illustrated, Rayleigh numbers for the collapse zone vary from 2380 for a height of 10 m to over 9500 for a height of 40 m. All Rayleigh numbers easily exceed the critical Rayleigh numbers associated with these drift heights. This suggests that heat transfer by convection will occur in the collapse zone overlying the drip shield during times when the waste package is generating significant heat.

It is not known how  $c_{conv}^*$  would scale to the size of a full-scale drift. Nonetheless, the average convection fitting parameter determined in these laboratory-scale tests (i.e.,  $\sim 0.024$  to  $0.027$ ) may be a reasonable first-order approximation for the repository scale in the absence of a site-specific convection fitting parameter.

## Conclusions

Heat transfer through a sample of crushed tuff from the Tptpll unit at Yucca Mountain was assessed for a variety of temperature regimes using a laboratory-scale apparatus. Once loaded into the test cell of the apparatus, the specimen was not disturbed, so differences in heat transfer due to packing were avoided. Measured heat flux and temperature were used to estimate the contributions to heat transfer by conduction, convection, and radiation.

Heat transfer was assumed to occur solely by conduction at low temperature gradients and low heat fluxes, the conditions at which the relationship between the temperature gradient and the heat flux is linear. Accordingly, a thermal conductivity of  $0.4 \text{ W/m-K}$  was measured for the Tptpll specimen at temperature gradients less than  $500^\circ\text{C/m}$  and heat fluxes less than  $250 \text{ W/m}^2$ . The contribution to heat transfer by radiation was calculated using principles developed from observations of packed bed experiments. These calculations indicated that radiation would not be a significant contributor to heat transfer through rubble unless the mean particle size and the temperature were sufficiently large. For the size distribution of the specimen tested in this study (assumed equivalent to  $\leq 0.001 \text{ m}$  diameter), heat flux by radiation was assumed to be

negligible (i.e.,  $< 5 \text{ W/m}^2$ ) even at the highest temperatures (up to  $173^\circ\text{C}$ ) and temperature gradients (i.e.,  $> 600^\circ\text{C/m}$ ) tested.

Heat transfer by convection was assumed to be that component of heat transfer that remained after conduction (calculated for a thermal conductivity of  $0.4 \text{ W/m-K}$ ) was removed from the total flux, and the contribution to heat transfer by radiation was determined to be negligible.

Based on this analysis, convection was only observed in the 0.15-m tall test cell at temperature gradients in excess of  $454$  to  $588^\circ\text{C/m}$ . Heat flux by convection exceeded 20% of the total heat flux only when the temperature gradient approached  $100^\circ\text{C/m}$ . The onset of convection observed during testing was consistent with the results of a Rayleigh number analysis that assumed the crushed tuff had a bulk permeability of  $1.0 \times 10^{-7} \text{ m}^2$ .

Analysis results of heat transfer observed during the laboratory-scale tests provide a means to estimate which heat transfer mechanisms would be active in geological HLW repository emplacement drifts that experience rockfall. The analogy is particularly relevant when the rubble has similar texture to the tested Ttptll specimen. If the rubble pile were comparable to the Ttptll sample tested, the relative contributions of conduction and radiation to heat transfer would be the same. The thermal conductivity of the bulk rubble pile would be  $0.4 \text{ W/m-K}$ , and heat transfer by radiation would be negligible.

The significantly larger convection cell size of the drift-scale collapse zone, however, would allow for greater convection compared with the laboratory-scale apparatus. In particular, the large Rayleigh number for the collapsed emplacement drift would more than offset a larger

critical Rayleigh number representative of an aspect ratio of drift width to drift height less than unity. This analysis suggests that heat transfer by convection would be expected in the collapse zone even for modest temperature gradients [i.e., a 50°C difference between the heat source and the top of a 40-m tall collapse zone (i.e., 1.25°C/m)]. Temperature differences of this magnitude are within the range of temperature gradients expected at the proposed Yucca Mountain geologic repository.

Additionally, results and scoping calculations from these analyses provide guidance on how the three heat transfer mechanisms (i.e., conduction, radiation, and convection) would vary for emplacement drifts with materials that exhibit physical characteristics and for systems with temperature regimes that differ from those tested.

## **Acknowledgements**

The authors thank Frank Dodge, Randy Fedors, Gordon Wittmeyer, Stuart Stothoff, and Erika Hanson whose careful reviews improved the quality of the document. Assistance by Paulette Houston in preparing the document is gratefully acknowledged.

This paper was prepared to document work performed by the Center for Nuclear Waste Regulatory Analyses (CNWRA) and its contractors for the U.S. Nuclear Regulatory Commission (NRC) under Contract No. NRC-02-02-012. The activities reported here were performed on behalf of the NRC Office of Nuclear Material Safety and Safeguards, Division of High-Level Waste Repository Safety. This paper is an independent product of CNWRA and does not necessarily reflect the view or regulatory position of NRC.

## References

Bear, J. (1972), *Dynamics of Fluids in Porous Media*, Dover Publications, New York.

Botterill, J.S., A.G. Salway, and Y. Toeman (1989), The effective thermal conductivity of high temperature particulate beds—II, Model predictions and the implication of the experimental values, *Int. J. Heat Mass Transfer*, 32(3), 595–609.

Brodsky, N.S., C.L. Howard, R.S. Taylor, and J.T. George (2003a), Field thermal conductivity measurements in the Topopah Spring Lower Lithophysal Unit, presented at the 11th International High-Level Radioactive Waste Management Conference (IHLRWM), American Nuclear Society, Las Vegas, Nevada, 30 March–2 April.

Brodsky, N.S., D.R. Bronowski, and C.L. Howard (2003b), Laboratory thermal conductivity testing for the Topopah Spring Lower Lithophysal Unit, presented at the 11th International High-Level Radioactive Waste Management Conference (IHLRWM), American Nuclear Society, Las Vegas, Nevada, 30 March–2 April.

Connor, C.B., P.C. Lichtner, F.M. Conway, B.E. Hill, A.A. Ovsyannikov, I. Federchenko, Y. Doubik, V.N. Shapar, and Y.A. Taran (1997), Cooling of an igneous dike 20 yr after intrusion. *Geology*, 25(8), 711–714.

CRWMS M&O (2001), Technical Update Impact Letter Report, MIS-MGR-RL-000001 Rev 00, CRWMS M&O, Las Vegas, Nevada.

DOE (2004), Multiscale Thermohydrologic Model, ANL-EBS-MD-000049, Rev 02, ICN 00, DOE, Washington, D.C.

Donaldson, I.G. (1970), The simulation of geothermal systems with a simple convective model. *Geothermics, Special Issue 2*, Vol. 2, Part 1, 649–654.

Freeze R.A. and J.A. Cherry (1979), *Groundwater*, Prentice Hall, Englewood Cliffs, New Jersey.

Green, R.T., F.T. Dodge, S.J. Svedeman, R.D. Manteufel, G. Rice, K.A. Meyer, and R.G. Baca (1995), Thermally driven moisture redistribution in partially saturated porous media, NUREG/CR-6348, U.S. Nuclear Regulatory Commission, Washington D.C.

Green, R.T., J.D. Prikryl, and M.E. Hill (1997), Assessment of heat flow through bulk geologic material, presented at the 24<sup>th</sup> International Thermal Conductivity Conference, Technomic Publ. Co., Pittsburgh, Pennsylvania, 26–29 October.

Gute, G.D., G. Ofoegbu, F. Thomassy, S. Hsiung, G. Adams, A. Ghost, B. Dasgupta, A.H. Chowdhury, and S. Mohanty (2003), MECHFAIL: A total-system performance assessment code module for evaluating engineered barrier performance under mechanical loading

conditions, CNWRA 2003-06, Center for Nuclear Waste Regulatory Analyses, San Antonio, Texas.

Kaviany, M. (1995), *Principles of Heat Transfer in Porous Media*, Springer, New York.

Lappin, A.R. (1980), Thermal conductivity of silicic tuffs: Predictive formalism and comparison with preliminary experimental results, SAND80-0769, Sandia National Laboratories, Albuquerque, New Mexico.

Lappin, A.R. and F.B. Nimick (1985), Bulk and thermal properties of the functional tuffaceous beds in holes USW G-1, UE-25a#1, and USW G-2, Yucca Mountain, Nevada, SAND82-1434, Sandia National Laboratories, Albuquerque, New Mexico.

Lappin, A.R., R.G. van Buskirk, D.O. Enniss, S.W. Butters, F.M. Prater, C.S. Muller, and J.L. Bergosh (1982), Thermal conductivity, bulk properties, and thermal stratigraphy of silicic tuffs from the upper portion of hole USW-G1, Yucca Mountain, Nye County, Nevada, SAND81-1873, Sandia National Laboratories, Albuquerque, New Mexico.

Lapwood, E.R. (1948), Convection of a fluid in a porous medium, *Proceedings of Cambridge Philosophical Society*, Vol. 44.

Mills, A.F. (1995), *Basic Heat and Mass Transfer*, Irwin, Chicago, Illinois.

Mongano, G.S., W.L. Singleton, T.C. Moyer, S.C. Beason, G.L.W. Eatman, A.L. Albin, and R.C. Lung (1999), Geology of the ECRB Cross Drift—Exploratory Studies Facility, Yucca Mountain Project, Yucca Mountain, Nevada, U.S. Geological Survey Bureau of Reclamation, Washington, D.C.

Nimick, F.B. (1990a), The thermal conductivity of the Topopah Spring Member at Yucca Mountain, Nevada, SAND86-0090, Sandia National Laboratories, Albuquerque, New Mexico.

Nimick, F.B. (1990b), The thermal conductivity of the seven thermal/mechanical units at Yucca Mountain, Nevada, SAND88-1387, Sandia National Laboratories, Albuquerque, New Mexico.

Nimick, F.B. and A.R. Lappin (1985), Thermal conductivity of silicic tuffs from Yucca Mountain and Ranier Mesa, Nye County, Nevada, SAND83-1711J, Sandia National Laboratories, Albuquerque, New Mexico.

Ofoegbu, G.I., B. Dasgupta, and K.J. Smart (2004), Thermally induced rock stress and implications for degradation of emplacement drifts at the potential Yucca Mountain nuclear waste repository, CNWRA 2004-06, Center for Nuclear Waste Regulatory Analyses, San Antonio, Texas.

Ryder, E.E., R.E. Finley, J.T. George, C.K. Ho, R.S. Longenbaugh, and J.R. Connolly (1996), Bench-scale experimental determination of the thermal diffusivity of crushed tuff, SAND94-2320, Sandia National Laboratories, Albuquerque, New Mexico.

Sass, J.H. and A.H. Lachenburch (1982), Preliminary interpretation of thermal data from the Nevada Test Site, USGS OFR-82-973, U.S. Geological Survey, Washington, D.C.

Sass, J.H., A.H. Lachenburch, W.W. Dudley, Jr., S.S. Priest, and R.J. Monroe (1988), Temperature, thermal conductivity, and heat flow near Yucca Mountain, Nevada. USGS OFR-87-649, U.S. Geological Survey, Washington, D.C.

Singh, A.K. and D.R. Chaudhary (1992), Experimental investigation on the thermophysical properties of moist porous materials, *Heat Recovery Systems & CHP (Combined Heat and Power)*, 12(2), 113–121.

White, F.M. (1988), *Heat and Mass Transfer* Addison-Wesley Publishing Co., New York.

Witherspoon, P.A., S.P. Neuman, M.L. Sorey, and M.J. Lippmann (1975), Modeling Geothermal Systems, *Il Fenomeno Geotermico E Sue Applicazione*, Atti dei Convegni Linsei, Roma.

## List of Figures

Figure 1. Photograph of the apparatus fabricated to measure thermal conductivity of bulk materials under steady-state conditions

Figure 2. Schematic of the steady-state, bulk thermal conductivity test apparatus

Figure 3. Measured heat flux versus temperature gradient for the 12 tests. The straight line denotes a linear relationship between heat flux and temperature gradient at low temperature gradients. The standard deviation of heat flux measured by the eight heat flux sensors is included as an error bar for each test.

Figure 4. Heat transfer by radiation versus temperature gradient for particle sizes 0.00001 m to 0.06 m

Figure 5. Heat transfer by radiation versus temperature gradient for particle sizes 0.00001 m to 0.001 m

Figure 6. Heat flux by convection ( $\text{W}/\text{m}^2$ ) plotted versus the temperature gradient [plotted as  $(\nabla T)^{5/4}$ ]

Figure 7. Heat flux by convection ( $\text{W/m}^2$ ) plotted versus the average temperature of the upper and lower test boundaries. Only data with a temperature gradient  $(\nabla T)^{5/4}$  greater than 2500 plotted.

Figure 8. The calculated convection fitting parameter plotted versus temperature gradient expressed as  $(\nabla T)^{5/4}$ . Test 1, with a convection fitting parameter value of  $\Theta 0.346$ , is not included in this plot.

Figure 9. Illustration of the drift void and drift designation area (taken from Gute et al., 2003)

Figure 10. The critical Rayleigh number plotted versus the height of the collapsed drift

Figure 11. Rayleigh number calculated for a drift with a temperature difference of  $50^\circ\text{C}$  between the heat source at the base and the top of the drift. The critical Rayleigh number is represented by the square series, and the Rayleigh number for the drift is represented by the diamonds.

## **List of Tables**

Table 1. Average bottom, average top, and average temperatures and temperature gradient (calculated using the average temperature)

Table 2. Summary of the average heat flux at the bottom and top boundaries, difference in the average heat fluxes (i.e., top-bottom), average heat flux, thermal conductivity, and variance in thermal conductivity

Table 3. The total measured heat flux (average of top and bottom boundary), calculated heat flux attributed to conduction, calculated heat flux attributed to convection, difference in heat flux measured at the top and bottom boundaries, and calculated convection coefficient

**Table 1. Average bottom, average top, and average temperatures and thermal gradient (calculated using the average temperature)**

Test Number	Bottom Temperature (°C)	Top Temperature (°C)	Average Temperature (°C)	Temperature Gradient (°C/m)
1	95.5	12.6	54.1	552.8
2	55.7	7.0	31.3	324.7
3	37.6	5.1	21.4	216.3
4	76.9	8.8	42.8	453.9
5	101.4	13.2	57.3	588.1
6	131.3	16.5	73.9	765.2
7	160.7	21.7	91.2	926.6
8	67.8	23.0	45.4	299.0
9	41.6	18.0	29.8	157.1
10	92.9	20.1	56.5	484.9
11	129.3	22.0	75.6	714.9
12	173.4	24.2	98.8	995.3

**Table 2. Summary of the average heat flux at the bottom and top boundaries, difference in the average heat fluxes (i.e., top-bottom), average heat flux, thermal conductivity, and variance in thermal conductivity**

Test Number	Bottom $Q$ (W/m <sup>2</sup> )	Top $Q$ (W/m <sup>2</sup> )	$\Delta Q$ (W/m <sup>2</sup> )	Average $Q$ (W/m <sup>2</sup> )	Thermal Conductivity (W/m-K)	Variance in Thermal Conductivity
1	266.8	258.1	-8.7	262.5	0.479	0.049
2	134.4	126.8	-7.6	130.7	0.409	0.042
3	83.7	77.0	-6.8	80.4	0.383	0.040
4	180.7	175.3	-5.4	178.0	0.432	0.044
5	239.1	245.8	6.8	242.5	0.458	0.047
6	319.4	352.6	33.3	335.9	0.498	0.051
7	398.4	467.3	68.9	432.8	0.545	0.056
8	115.5	115.9	0.4	115.7	0.426	0.044
9	58.1	52.4	-5.7	55.2	0.387	0.040
10	186.6	205.7	19.1	196.2	0.452	0.047
11	292.9	325.5	32.6	309.1	0.486	0.050
12	421.9	509.5	87.5	469.5	0.557	0.057

**Table 3. The total measured heat flux (average of top and bottom boundary), calculated heat flux attributed to conduction, calculated heat flux attributed to convection, difference in heat flux measured at the top and bottom boundaries, and calculated convection coefficient**

Test Number	Measured $Q_{total}$ (W/m <sup>2</sup> )	Calculated $Q_{cond}$ (W/m <sup>2</sup> )	$Q_{conv}$ (W/m <sup>2</sup> )	$\Delta Q$ (W/m <sup>2</sup> )	$c^*_{conv}$
1	262.5	221.1	41.4	-8.7	-0.346
2	130.7	129.9	0.8	-7.6	-0.001
3	80.4	86.5	-6.1	-6.8	0.003
4	178.0	181.6	-3.5	-5.4	0.005
5	242.5	235.2	7.3	6.8	0.076
6	335.9	306.1	29.9	33.3	0.024
7	432.8	370.6	62.2	68.9	0.027
8	115.7	119.6	-3.9	0.4	0.002
9	55.2	62.8	-7.6	-5.7	0.003
10	196.2	193.9	2.3	19.1	-0.004
11	309.1	285.9	23.2	32.6	0.026
12	469.5	398.1	71.4	87.5	0.026



**Figure 1. Photograph of the apparatus fabricated to measure thermal conductivity of bulk materials under steady-state conditions**

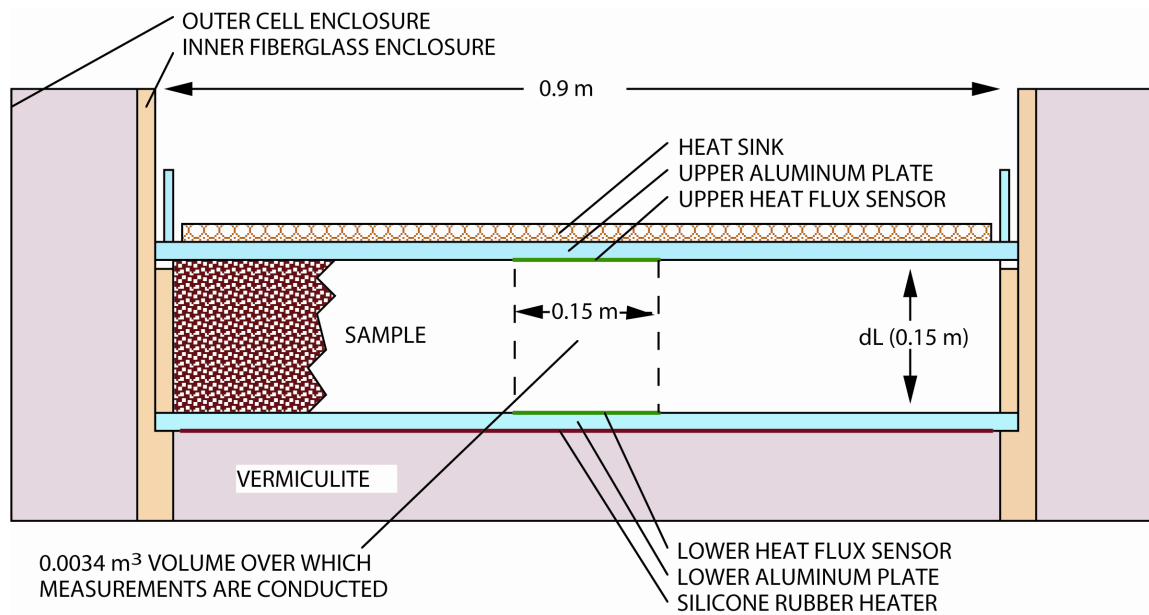


**Figure 2. Schematic of the steady-state, bulk thermal conductivity test apparatus**

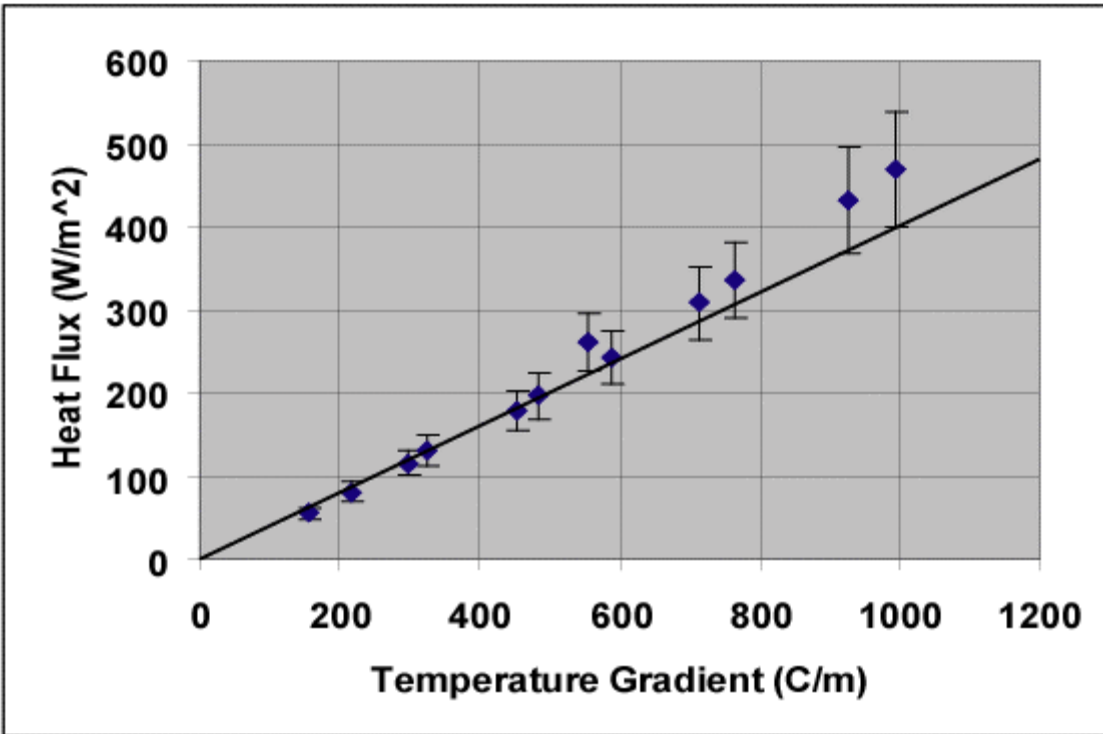


**Figure 3. Measured heat flux versus temperature gradient for the 12 tests. The straight line denotes a linear relationship between heat flux and temperature gradient at low temperature gradients. The standard deviation of heat flux measured by the eight heat flux sensors is included as an error bar for each test.**

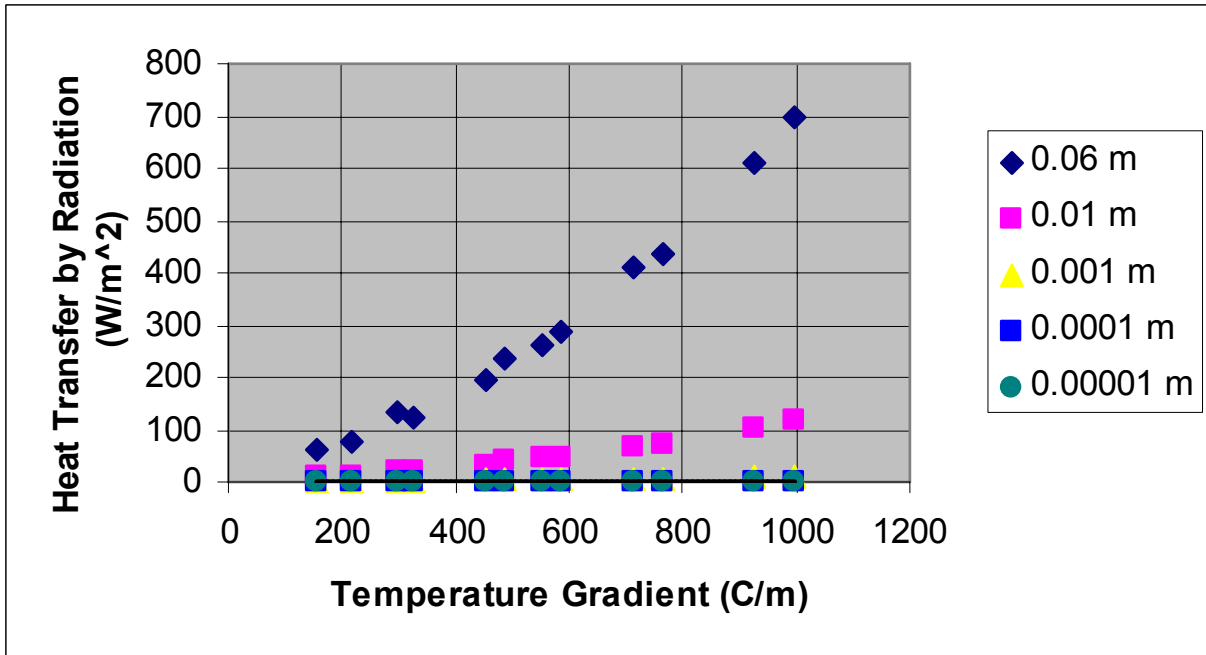


**Figure 4. Heat transfer by radiation versus temperature gradient for particle sizes 0.00001 m to 0.06 m**

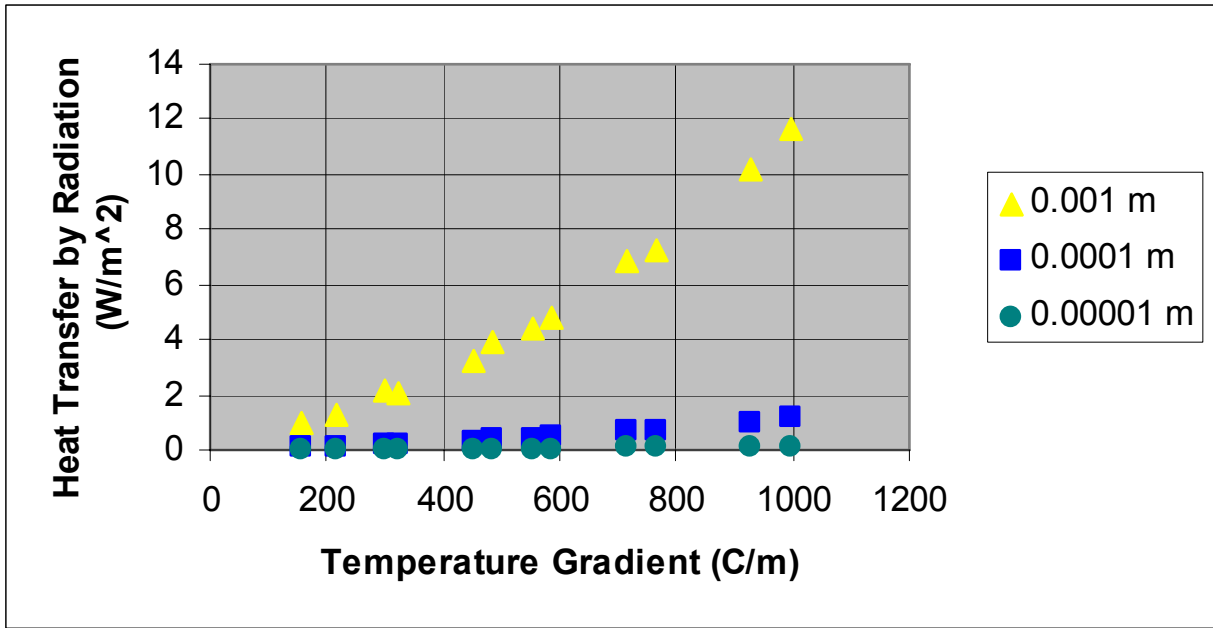


**Figure 5. Heat transfer by radiation versus temperature gradient for particle sizes 0.00001 m to 0.001 m**

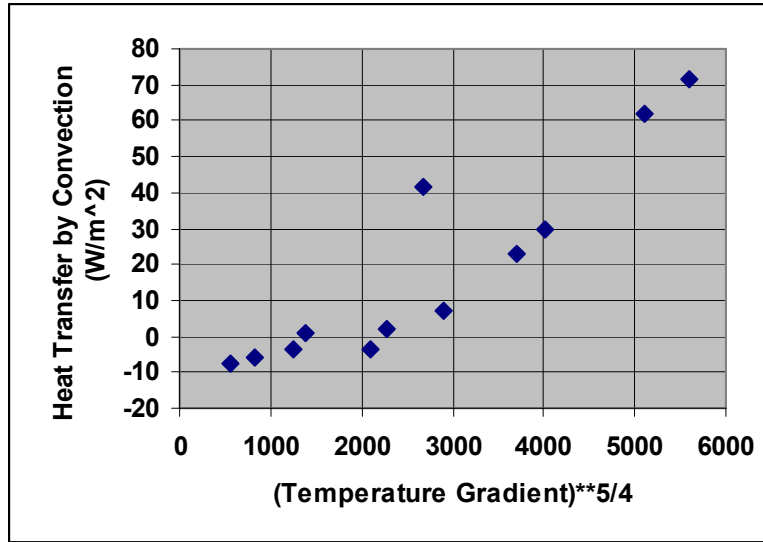
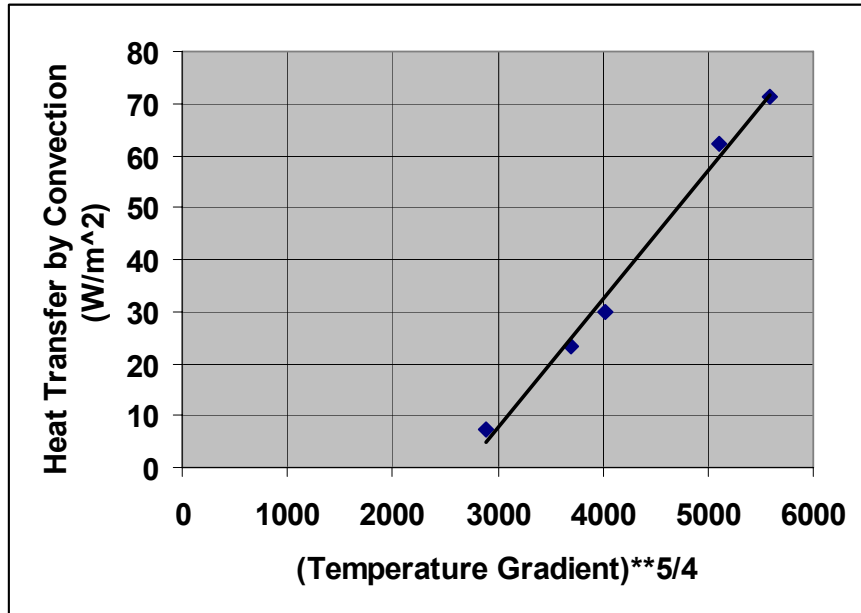
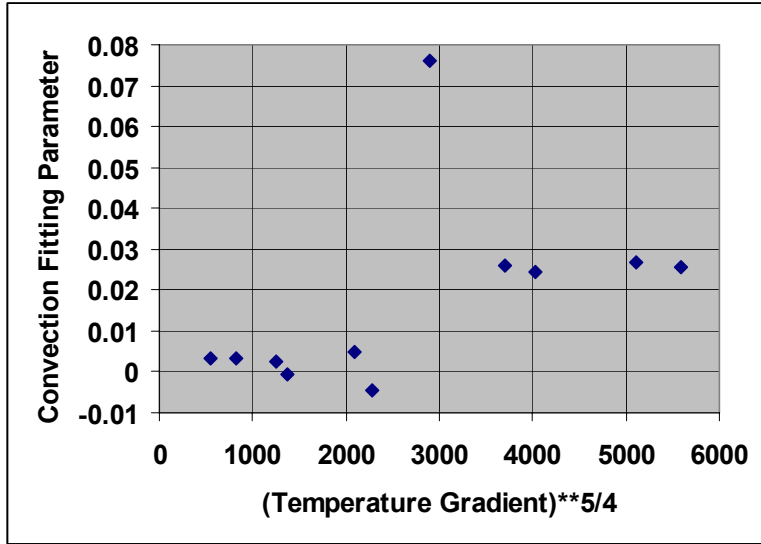


Figure 6. Heat flux by convection (W/m<sup>2</sup>) plotted versus the temperature gradient [plotted as  $(\nabla T)^{5/4}$ ]



**Figure 7. Heat flux by convection ( $\text{W}/\text{m}^2$ ) plotted versus the average temperature of the upper and lower test boundaries. Only data with a temperature gradient  $(\nabla T)^{5/4}$  greater than 2500 plotted.**



**Figure 8. The calculated convection fitting parameter plotted versus temperature gradient expressed as  $(\nabla T)^{5/4}$ . Test 1, with a convection fitting parameter value of  $\Theta 0.346$ , is not included in this plot.**

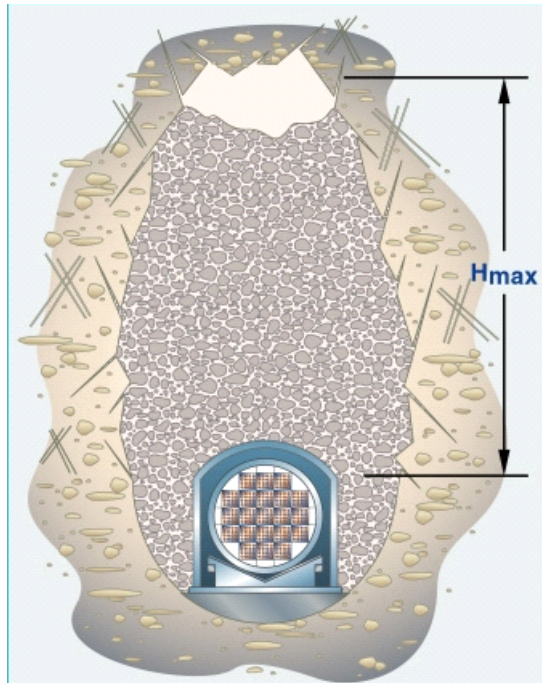


**Figure 9. Illustration of the drift void and drift designation area (taken from Gute et al., 2003)**

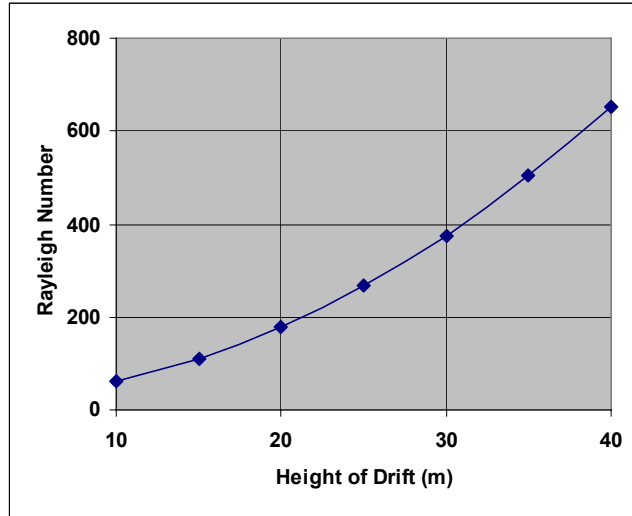


**Figure 10. The critical Rayleigh number plotted versus the height of the collapsed drift**

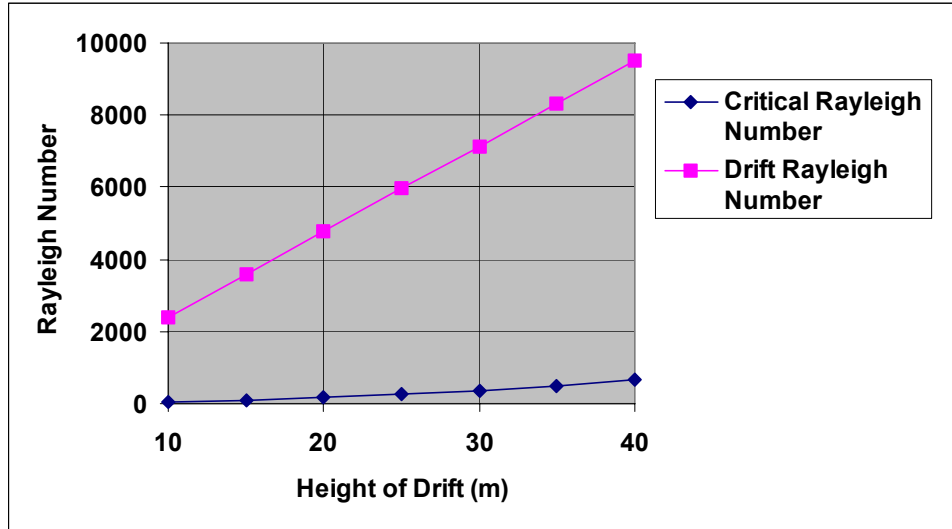


**Figure 11.** Rayleigh number calculated for a drift with a temperature difference of 50°C between the heat source at the base and the top of the drift. The critical Rayleigh number is represented by the square series, and the Rayleigh number for the drift is represented by the diamonds.